JOURNAL OF SOLID STATE CHEMISTRY 36, 331–338 (1981)

Crystal Growth and Electrical Properties of Lithium, Rubidium, and Cesium Molybdenum Oxide Bronzes

PIERRE STROBEL* AND MARTHA GREENBLATT†

Department of Chemistry, Rutgers University, New Brunswick, New Jersey 08903

Received March 20, 1980; in revised form May 26, 1980

Crystals of $Li_{0.33}MoO_3$ (blue), $Rb_{0.23}MoO_3$ (blue) and $Cs_{0.31}MoO_3$ (red) were grown by electrolysis from MoO_3–M_2MoO_4 melts (M = alkali metal) with composition 70–77 mole% MoO_3. Melts richer in M_2MoO_4 produced MoO_2 only. Correlation is made between bronze formation and the coordination of Mo in the melt and in the equilibrium solid phase $M_2Mo_4O_{13}$. $Li_{0.33}MoO_3$ and $Cs_{0.31}MoO_3$ are semiconductors with high-temperature-range activation energies 0.16 and 0.12 eV. $Rb_{0.23}MoO_3$ has an electrical behavior similar to that of blue K_xMoO_3 with a semiconductor–metal transition at (170 ± 5) K. ESR spectra observed in $Li_{0.33}MoO_3$ and $Rb_{0.23}MoO_3$ single crystals at 4.2 K show extensive delocalization of the $4d^1$ electron associated with Mo(V) centers. Attempts to grow molybdenum bronzes containing Ca or Y were unsuccessful.

Introduction

The molybdenum oxide bronzes M_xMoO_3 (where M is an electropositive element) have attracted much attention because of their structural and electrical properties (*1*, *2*) Unlike tungsten bronzes, most known molybdenum bronze phases have layer structures and are semiconducting. Of particular interest is the semiconductor–metal transition observed in blue K_xMoO_3 (*3*). Similar behavior might be expected for the isostructural phase Rb_xMoO_3 prepared by Reau *et al.* (*4*), but no single-crystal electrical study was available on this phase. In the system Li–Mo–O, Reau *et al.* (*5*) prepared two bronze phases, for which neither crystal growth nor physical studies were available. In the system Cs–Mo–O, crystals of a red bronze Cs_xMoO_3 have been obtained by Reid and Watts (*6*). From structural considerations, Mumme and Watts (*7*) suggested that this material might be a better conductor than the blue potassium bronze, but no electrical measurements have been reported.

Electron spin resonance (ESR) investigations of single crystals of red and blue K molybdenum bronzes have shown the presence of unpaired d electrons associated with Mo(V) centers (*8*, *9*).

The aim of this study was (1) to investigate systematically conditions of the electrolytic process which allows the crystal growth of Li, Rb, and Cs molybdenum bronzes; (2) to determine by single-crystal measurements the electrical transport prop-

* Present address: National Research Council, Division of Chemistry, Ottawa KIA OR6, Canada.

† To whom all correspondence should be addressed.

0022-4596/81/030331-08$02.00/0

erties of the Li, Rb, and Cs bronze phases; (3) to observe and characterize by electron spin resonance the electronic properties of Mo(V) centers in these systems.

In addition, we have attempted to grow single crystals of molybdenum bronzes containing calcium and yttrium by the electrolytic technique, as these phases are known to form tungsten bronzes by electrolysis (*10*).

Experimental

The crystal growth of molybdenum bronzes was performed in an electrolytic cell shown in Fig. 1. A 100-ml high-purity alumina crucible with inner cylindrical compartment and two platinum electrodes was placed in a long Mullite tube in a vertical tubular furnace. The cathode was centered by an alumina guide, which could be raised or lowered into the crucible from the top of the tube. The extremities of the vessel were designed to allow evacuating to ~0.01 Torr or flushing with an inert gas.

Starting materials were reagent grade Li_2MoO_4, $CaMoO_4$, Rb and Cs carbonates, MoO_3, and Y_2O_3. Rb and Cs molybdates were prepared by heating stoichiometric mixtures of alkali carbonate and molybdenum trioxide in a dry nitrogen stream at 750°C for 15 hr.

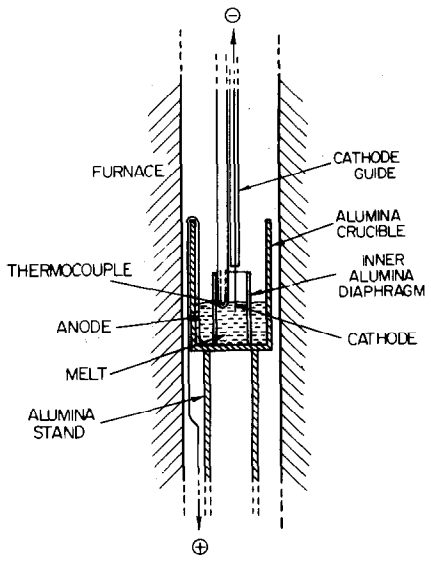

FIG. 1. Electrolysis cell.

In a typical electrolysis run, the sample charge (40–60 g) was intimately mixed, placed in the crucible, and outgassed overnight under vacuum at a temperature close to the melting point. The vessel was then flushed with dry nitrogen (1 atm) and brought to a temperature slightly above the melting point. The cathode was lowered ~10 mm below the melt surface, and a controlled current (<10 mA) was passed through the cell for several days. At the end of the process, the cathode was raised above the melt before cooling. Crystals were usually found both on the cathode and in the charge. They were recovered by soaking the crucible in hot dilute HCl. Crystals were identified and oriented by X-ray diffraction single-crystal (Precession camera) and powder techniques (Norelco diffractometer using nickel-filtered copper radiation). The alkali metal content was determined by atomic absorption spectometry on samples dissolved in aqua regia.

Electrical resistivities were measured on platelet-like crystals by the Van der Pauw technique (*11*) and on needle-shaped samples (lithium bronze) by a collinear four-probe arrangement. Voltage drop across high-resistivity samples were measured using a Keithley 610 electrometer. Ohmic contacts to the crystals were obtained with ultrasonically applied indium. Electron spin resonance spectra were taken with an X-band coherent superheterodyne spectrometer operating in the absorption mode and using field modulation. The Klystron frequency was ~9000 MHz.

Results

Crystals Growth

The conditions and results of electrolysis

are summarized in Table I. Early attempts produced only MoO_2. As emphasized in previous works on K and Cs bronzes (*6, 12*) both temperature and composition of the melt appeared to be critical parameters.

In the Li–Mo–O system (Fig. 4) bronze formation was not obtained at the lowest eutectic composition (run B), but near the $Li_2Mo_4O_{13}$ composition melting at ~560°C (run A). The temperature had to be kept very close to the solidification temperature, since lithium molybdenum bronzes are not stable above 590°C (*5*). In runs C and D phosphate was added with the intention of preparing new mixed phosphate Mo^{5+} phases. Addition of phosphate did not lower the melting point significantly or yield other phases. A rubidium bronze was also obtained near the $Rb_2Mo_4O_{13}$ composition. In the Cs–Mo–O system, a composition change from 28.0 to 34.8 mole% Cs_2MoO_4 produced a system out of the bronze crystallization range (runs F and G).

During the electrolysis, evolution of I and V through the cell showed interesting features. The growth of a crystal on the cathode increases the surface area of the

TABLE I

RESULTS OF ELECTROLYSIS CRYSTAL GROWTH

No.	Melt Composition	Melt mole%	Temp. (±5) (°C)	Current (±0.2) (mA)	Voltage drop start → end (V)	Duration (Days)	Crystals obtained
A	MoO_3 Li_2MoO_4	70.6 29.4	560	6.7	1.0 → 0.8	4	Bulky black crystals MoO_2 Dark blue needles, Li_xMoO_3, 2–6 mm long
B	MoO_3 Li_2MoO_4	50.5 49.5	560	6.8	1.7 → 0.6	6	MoO_2 only
C	MoO_3 Li_2O P_2O_5	50.8 41.2 8.0	580	6.4	0.9 → 0.8	5	MoO_2 + Li_xMoO_3, 3–6 mm long
D	MoO_3 Li_2O P_2O_5	53.3 35.0 21.8	550	6.9	1.0 → 0.3	10	MoO_2 only
E	MoO_3 Rb_2MoO_4	75.8 24.2	570	6.7	1.5 → 1.3	6	Dark blue crystals Rb_xMoO_3 3–8 mm long
F	MoO_3 Cs_2MoO_4	65.2 34.8	540	7.0	1.2	6	Reddish crystals MoO_2 (see text)
G	MoO_3 Cs_2MoO_4	72.0 28.0	550	6.9	1.4	10	Bulky reddish crystals MoO_2 Red plates Cs_xMoO_3, 1–4 mm long
H	MoO_3 $CaMoO_4$	81.0 19.0	735	6.7	0.70 → ~4	2	Polycrystalline $CaMoO_4$ deposit on cathode
I	MoO_3 Y_2O_3	90.3 9.7	755	6.6	1.7 → 3.2	4	MoO_2 only

cathode; if the crystal is a good electric conductor this results in a decrease of current density at constant current, and an accompanying decrease of potential (*13*). Such an effect was particularly noticeable in runs B and D, where a large decrease in V seemed related to extensive formation of MoO_2, which is a metallic conductor.

In the Li and Cs molybdate melts, bronze and molybdenum dioxide were obtained simultaneously. The crystals were easily separated according to their habit. In the Cs system MoO_2 crystals, unambiguously identified by their X-ray diffraction pattern, showed an unusual red or bronze shine. This had been observed previously by Reid and Watts (*6*). Since their deposition was not accompanied by the expected voltage decrease, we believe that they may contain surface defects or a thin surface layer of red cesium bronze.

Electrolysis was carried out in the system Ca–Mo–O and Y–Mo–O near the molybdenum-rich eutectic, which occurred at 25 mole% $CaMoO_4$ at 727°C, and 10 mole% Y_2O_3 at 740°C (*14*), respectively. No bronzes were obtained, and the experiments could not be carried out for an extended period of time because of significant sublimation of MoO_3 in this temperature range.

Characterization of Crystals

From X-ray and chemical analysis, the bronzes grown were identified as $Li_{0.33}MoO_3$, monoclinic, same phase as in (*5*); $Rb_{0.23}MoO_3$, monoclinic, same blue phase as in (*4*); and $Cs_{0.31}MoO_3$, monoclinic, same red phase as in (*6*). The alkali metal content is in fairly good agreement with previously reported homgeneity ranges: $0.31 \leq x \leq 0.39$ for the lithium phase (*5*), $0.24 \leq x \leq 0.30$ for the blue rubidium phase (*4*), and 0.33 (*6*) or 0.25 (*7*) for the cesium phase.

All crystals were obtained as needles or plates with the long dimension parallel to the *b* axis. The red $Cs_{0.31}MoO_3$ crystals had a tendency to twin and seemed to undergo a phase transition upon grinding. They turned from red to blue, and yielded an X-ray powder pattern which did not correspond to the red phase. This pattern (Table II) could not be indexed on the basis of known potassium or rubidium bronze phases.

Electrical Resistivity

Electrical resistivities were measured in the range 77–300 K along the *b* axis for Li_xMoO_3, and in a plane containing *b* for Rb_xMoO_3 and Cs_xMoO_3.

The room-temperature resistivities were of the order of 5 Ω cm for Li_xMoO_3 and 10^5 Ω cm for Cs_xMoO_3. Both compounds showed typical semiconducting behavior (Fig. 2). Their activation energies in the high-temperature region were 0.16 and 0.12 eV, respectively.

The blue rubidium molybdenum bronze had a much lower resistivity, 8×10^{-3} Ω cm at room temperature. The temperature variation of the resistivity (Fig. 3) shows a sharp break at (170 ± 5)°C corresponding to a semiconductor–metal transition. The resistivity was practically temperature independent above the transition. In

TABLE II

X-RAY DATA FOR GROUND Cs_xMoO_3 (BLUE POWDER)

d	*I*	*d*	*I*	*d*	*I*
7.9	60	2.926	30	1.971	10
5.15	10	2.864	5	1.961	10
4.62	20	2.855	5	1.932	20
4.48	5	2.503	20	1.850	5
3.484	100	2.428	<5	1.843	5
3.470	100	2.345	5	1.723	5
3.247	30	2.310	5	1.688	5
3.187	20	2.098	10	1.626	10
3.087	40	2.019	20		
3.005	25	1.978	10		

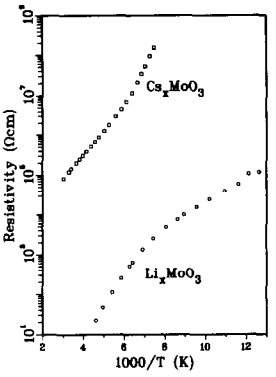

FIG. 2. Resistivity versus reciprocal temperature for single-crystal samples of blue $Li_{0.33}MoO_3$ (measurement along b) and red $Cs_{0.31}MoO_3$ (measurement in a plane containing b).

the semiconducting region the activation energy was ~0.04 eV in the range 77–130 K.

ESR Measurements

Electron spin resonance was measured in single crystals of $Li_{0.31}MoO_3$ and $Rb_{0.23}MoO_3$ with the external magnetic field in the ac plane for each, respectively. No ESR was observed at room- or liquid nitrogen temperatures for either crystal. At 4.2 K broad ($\Delta H \sim 30$ G), structureless asymmetrical, and nearly orientation independent lines at $g = 1.93$ and $g = 2.1$ were detected in the lithium bronze. The ESR spectra of $Rb_{0.23}MoO_3$ at 4.2 K showed three broad ($\Delta H \sim 7$ to 14 G) structureless lines similar to those of the ESR spectra observed under similar conditions in blue potassium bronze (*9*). The positions of ESR lines vary with orientation and the g values of all three signals are between $g = 1.95$ and $g = 1.88$ with rotation of H about the b axis. Hyperfine structure due to the ~25% abundant isotopes of ^{95}Mo and ^{97}Mo with $I = \frac{5}{2}$ could not be resolved in either sample. The crystals of red Cs_xMoO_3 were not large enough for the ESR investigation. Work is now in progress to grow larger crystals for an ESR study of this phase.

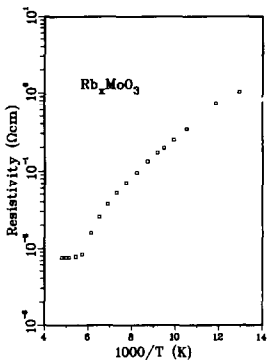

FIG. 3. Resistivity versus reciprocal temperature for single-crystal sample of blue $Rb_{0.23}MoO_3$ (measurement in a plane containing b).

Discussion

Bronze Formation

Figure 4 summarizes the various compositions at which attempts were made to grow molybdenum bronze single crystals by electrolysis. It can be seen that for any alkali metal M, bronzes have been obtained only in a narrow range of melt composition, between 70 and 77 mole% MoO_3, corresponding to a ratio M/Mo 0.6 to 0.45. The

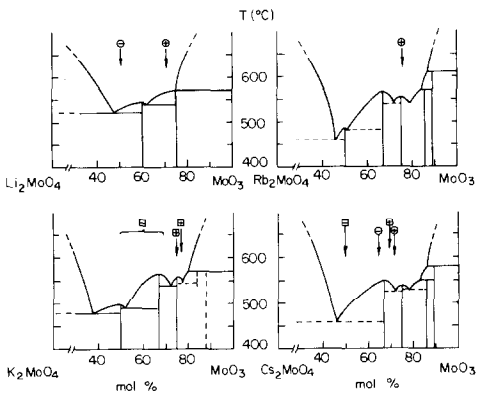

FIG. 4. Comparisons of electrolytic growth conditions for Li, K, Rb, and Cs molybdenum bronzes. ⊕, bronze obtained this work; ⊞, bronze obtained Refs. (*6*, *12*); ⊖, MoO_2 obtained this work; ⊟, MoO_2 obtained Refs. (*6*, *12*). Phase diagrams were taken from Ref. (*14*).

bronzes have common structural features: (i) they contain six-coordinated molybdenum only, (ii) for M = K, Rb and Cs they consist of units of edge-sharing molybdenum octahedra (6 octahedra in red bronzes, 10 octahedra in blue bronzes) (*2*). Bronze formation is certainly favored if similar groups are present in the molybdate melt. Stephenson and Wadsley (*15*) suggested that large anions such as $(Mo_6O_{22})^{8-}$, found in molybdenum isopolyacids, might be present in the fused salt systems M_2MoO_4–MoO_3. The actual structure of atomic groups in the melt is unknown, but one can reasonably assume that, at temperatures close to the solidification point, structural units in the liquid and solid phases are similar (*16*). Further arguments supporting this view are (i) the small melting entropy of alkali molybdates (~10 cal mole^{-1} K^{-1}) (*17*); (ii) ir studies on glasses formed by rapid quenching of molten $M_2Mo_2O_7$ (*18*), which show mixed molybdenum coordinations 4 and 6 as in crystalline $M_2Mo_2O_7$ (*19*).

As pointed out by Gatehouse and Leverett (*20*) for the potassium phases, the structures of alkali molybdates present a remarkable change as the ratio M/Mo decreases from 2 to 0. The coordination of molybdenum is 4 in M_2MoO_4, 4 and 6 in $M_2Mo_2O_7$, 5 and 6 in $M_2Mo_3O_{10}$, 6 only in $M_2Mo_4O_{13}$ (*17, 20*). In the latter structures, extensive edge sharing occurs between the molybdate octahedra. Accordingly, the bronze phases, which require similar structural conditions, are obtained only from melts of composition close to $M_2Mo_4O_{13}$.

Structures

The lithium molybdenum bronze was found to be monoclinic on the basis of its X-ray diffraction powder pattern by Reau *et al.* (*5*), but no description of the structure based on single-crystal X-ray diffraction analysis has been reported. In the Cs_xMoO_3 bronze, we observed a phase transformation (associated with a change in color) upon grinding, i.e., under pressure. The existence of other cesium molybdenum bronze phases should not be surprising, since different blue and red phases with approximately equal values of x exist for potassium and rubidium (*4, 12*). Furthermore, blue K molybdenum bronzes, with structures differing from phases prepared by electrolysis, have been obtained under high pressure (*21*). Further study on the lithium and cesium bronze structures is in progress and will be reported in due course.

Electrical Resistivity

The electrical behavior of Rb_xMoO_3 is similar to that of the isostructural phase K_xMoO_3 (blue), where a semiconductor–metal transition occurs at 180 K (*12, 22*). In the semiconducting region, the two phases exhibit similar curvatures in the plot of log ρ vs T^{-1}, which may be due to variable-range hopping (*23*). The observed activation energy is of the same order of magnitude in both phases.

The potassium and rubidium blue bronzes contain clusters of 10 edge-sharing molybdenum octahedra, in contrast to the red potassium and cesium bronzes where the basic unit is made up of 6 octahedra. Bouchard *et al.* (*22*) attributed the difference in the electrical behavior of blue and red bronzes to differences in molecular orbital population and electron delocalization over the $(Mo_{10}O_{30})$ and (Mo_6O_{18}) clusters. Mumme and Watts (*7*) pointed out the difference in cluster stacking between potassium and cesium red bronzes. In the potassium phase clusters share only corners, whereas in the cesium phase they share edges building infinite chains along the b axis. Mumme and Watts suggested that this stacking might result in considerable electron delocalization and corresponding low resistivity in Cs_xMoO_3. This was

not confirmed experimentally. The room-temperature resistivity ρ of Cs_xMoO_3 (10^5 Ωcm) is comparable to that of red K_xMoO_3 (2×10^4 Ωcm) (*12*). Furthermore, if, like Bouchard *et al.* (*22*), one assumes a hopping mechanism for conductivity in the red bronzes, the density of charge carriers n is constant and equal to the density of electrons transferred to the (MoO_3) network by the insertion of the alkali atoms. In Cs_xMoO_3, $n = 4.7 \times 10^{21}$ cm^{-3}, and the mobility at room temperature is $\mu = (ne\rho)^{-1} \simeq 10^{-8}$ cm^2 V^{-1} sec^{-1}. Such a low value of μ does not support the large delocalization expected on the basis of the crystal structure.

In the lithium bronze $Li_{0.33}MoO_3$ the resistivity is intermediate between "red" and "blue" bronzes. In this phase there seems to be a change in conduction mechanism at $\sim$140 K as the activation energy drops from 0.16 eV in the high-temperature region to 0.06 eV in the low-temperature region. Further discussion will be possible after a complete determination of the structure.

Electron Spin Resonance

Results of the ESR measurements on the Li and Rb molybdenum bronzes show the presence of unpaired d^1 electrons at low temperature. The measured g factors are comparable to the g values observed in red and blue K molybdenum bronzes (*9*) and are attributed to d^1 electrons whose ground state consists mainly of d_{xy} wavefunctions (*24*) associated with Mo(V) octahedral centers with extensive delocalization of the d^1 electron over several molbdenum sites. There appears to be much more extensive delocalization in the blue bronzes which have units of 10 M–O octahedra than in the red bronzes, where the basic unit of structures is edge sharing 6 M–O octahedra. Due to the generally poor quality of the spectra and complete lack of hyperfine data the extent of delocalization of the electrons in the blue bronzes cannot be determined.

Conclusion

Crystal growth of the bronze phase Li_xMoO_3 and Rb_xMoO_3 has been reported here for the first time. For all molybdenum bronzes, electrolytic crystal growth has been successful only in a narrow range of melt composition, corresponding to the starting solid phase $M_2Mo_4O_{13}$. It is likely that the formation of bronzes occurs due to the presence of the required structural groups in the melt as they are found in $M_2Mo_4O_{13}$, edge-sharing molybdenum octahedra. The blue rubidium bronze $Rb_{0.23}MoO_3$ exhibits a semiconductor metal transition at about 170 K similar to its potassium analog. Lithium and cesium molybdenum bronzes are semiconductors. The electrical behavior of red $Cs_{0.31}MoO_3$ is very similar to that of red potassium bronze, in spite of differences in the stacking of molybdenum octahedra. ESR spectra observed at 4.2 K in single crystals of $Li_{0.33}MoO_3$ and $Rb_{0.23}MoO_3$ show the presence of unpaired d^1 electrons associated with Mo(V) octahedral centers.

Acknowledgment

The authors wish to thank Professor J. H. Pifer for his help with the ESR measurements, Professor A. Wold for valuable discussions on the electrolytic process, and Drs. C. Hurd and S. P. McAlister for their help with the electrical measurements, which were performed at the National Research Council, Ottawa. This material is based upon work supported by the National Science Foundation under Grant DMR78-08554 and by the Rutgers University Research Council.

References

1. P. HAGENMULLER, *Progr. Solid State Chem.* **5**, 71 (1971).
2. P. G. DICKENS AND P. J. WISEMAN, *MTP Int. Rev. Sci., Inorg. Chem. Ser.* **10**, 211 (1975).
3. A. WOLD, *Bull. Soc. Chim. Fr.*, 1059 (1965).
4. J. M. REAU, C. FOUASSIER, AND P. HAGENMULLER, *Bull. Soc. Chim. Fr.*, 2883 (1971).

5. J. M. Reau, C. Fouassier, and P. Hagenmuller, *J. Solid State Chem.* **1,** 326 (1970).
6. A. F. Reid and J. A. Watts, *J. Solid State Chem.* **1,** 310 (1970).
7. W. G. Mumme and J. A. Watts, *J. Solid State Chem.* **2,** 16 (1970).
8. G. Bang and G. Sperlich, *Phys. Lett. A* **49,** 21 (1974).
9. G. Bang and G. Sperlich, *Z. Phys.* **1,** 1322, (1975).
10. W. Ostertag, *Inorg. Chem.* **5,** 758 (1966).
11. L. J. Van Der Pauw, *Philips. Res. Rep.* **13,** 1 (1958).
12. A. Wold, W. Kunnmann, R. J. Arnott, and A. Ferretti, *Inorg. Chem.* **3,** 345 (1964).
13. R. A. Fredlein and A. Danjanovic, *J. Solid State Chem.* **4,** 94 (1972).
14. E. M. Levin, C. R. Robbins, and H. F. McMurdie, "Phase Diagrams for Ceramists," Amer. Ceramic Soc., Columbus, Ohio, 1964, 1969, 1975.
15. N. C. Stephenson and A. D. Wadsley, *Acta Crystallogr.* **19,** 241 (1965).
16. A. R. Ubbelohde, "Melting and Crystal Structure," Oxford Univ. Press (Clarendon), London/New York, 1965.
17. M. G. Gmelins, *in* "Handbuch der anorganische Chemie," Vol. 53, B1, Chap. 7, Springer-Verlag, Berlin (1975).
18. R. G. Gossink and J. M. Stevels, *J. Non-Cryst. Solids* **5,** 217 (1971).
19. M. Seleborg, *Acta Chem. Scand.* **21,** 499 (1967).
20. B. M. Gatehouse and P. Leverett, *J. Chem. Soc. A,* 1398 (1968); 2107 (1971).
21. T. A. Bither, J. L. Gillson, and H. S. Young, *Inorg. Chem.* **5,** 1559 (1966).
22. G. H. Bouchard, J. Perlstein, and M. J. Sienko, *Inorg. Chem.* **6,** 1682 (1967).
23. N. F. Mott, *Phil. Mag.* **35,** 111 (1977).
24. T. Shimizu, *J. Phys. Soc. Japan* **23,** 848 (1967).